Waveguide-Based Refractometers Using Bulk, Long-and Short-Range Surface Plasmon Modes: Comparative Study

Anton V. Dyshlyuk, Oleg B. Vitrik, and Uliana A. Eryusheva

***Abstract*—We present a numerical study comparing three configurations of the waveguide-based surface plasmon resonance refractometer: without a buffer layer based on the excitation of the bulk surface plasmon mode, and with a buffer layer using the symmetric (long-range) and antisymmetric (short-range) plasmon modes. Optimal conditions ensuring the sharpest resonant dip in the refractometer's transmission spectrum are identified. Relative merits of various configurations in terms of the figure-of-merit parameter, local sensitivity to refractive index variations near the metal film, and the size of the sensing element are quantified and discussed.**

***Index Terms*—Biosensing, chemosensing, long-range surface plasmon mode, short-range surface plasmon mode, SPR, surface plasmon resonance, waveguide-based SPR-refractometer.**

I. Introduction

REFRACTOMETRIC sensors based on surface plasmon resonance (SPR) represent a topical trend in modern bio- and chemosensing technologies [1]–[4]. Sensors of this kind use resonant excitation of surface plasmon waves (coupled oscillations of free electron density and electromagnetic field bound to a metal-dielectric interface) to detect minute variations in refractive index induced by (bio)chemical reactions near the interface [4]–[6].

The most common configuration of the SPR-refractometer is the well-known Kretschmann scheme, in which surface plasmons are excited by a beam of light incident from within a prism on its metal-coated facet [4]–[6]. This configuration is widely used in laboratory-based biochemical researches, but it is not suited for making portable and inexpensive sensors, including disposable and point-of-care devices. Considerable research efforts, therefore, are devoted to the development of waveguide-based SPR-refractometers in which a surface plasmon mode (SPM) is excited by modes of a dielectric waveguide [5]–[14], [18], [19]. Sensors of this type, in contrast to the Kretschmann configuration, can be easily miniaturized and coupled to fiber and integrated optics elements, can be used for measurements in situ and in hard-to-reach locations, as well as aid in cost reduction of SPR bio- and chemosensing systems [7]–[11].

Among various types of waveguide-based SPR-refractometers known to date the simplest one is probably the waveguide analog of the Kretschmann scheme, in which a metal film is deposited directly onto the light-guiding core of a waveguide [5]–[8], [10], [14]. Other configurations have also been proposed, which use a buffer layer between the core and the metal film with the refractive index close to that of the ambient medium [8]–[10], [15]–[19]. In the latter case it is possible to make use of either symmetric (long-range) or antisymmetric (short-range) surface plasmon modes arising due to the hybridization of surface plasmon modes supported by different sides of a thin metal film [5], [6].

We should note that in the SPR-refractometer without a buffer layer, similarly to the Kretschmann scheme, the refractive index of the waveguiding layer is typically much larger than that of the ambient medium. This makes the propagation constants of the surface plasmon modes at two sides of the metal film quite different so that they cannot hybridize effectively even if the film is very thin. Hence, the plasmon mode excited in the SPR-refractometer without a buffer layer is localized at the metal | ambient medium interface and is very close in its characteristics to the SPM at the surface of a bulk metal. We shall thus refer to it as the 'bulk surface plasmon mode' (BSPM) as opposed to the symmetric surface plasmon mode (SSPM) and antisymmetric surface plasmon mode (ASPM) in the refractometer with a buffer layer.

Symmetric, antisymmetric and bulk plasmon modes differ in their propagation constants, losses, penetration depths and sensitivity to the ambient refractive index [6]. As to which of the modes is most suitable for building an SPR-refractometer there seems to be no apparent consensus in the published literature. Those authors who propose refractometers based on SSPM emphasize its lower losses and, correspondingly, a narrower resonant dip in the transmission spectrum as well as higher spectral sensitivity [15]–[17].

Manuscript received May 30, 2018; revised August 9, 2018; accepted September 2, 2018. The work was supported by the Russian Science Foundation under Grant 16-12-10165. *(Corresponding author: Anton V. Dyshlyuk.)*

A. V. Dyshlyuk is with the Far Eastern Federal University, Vladivostok 690090, Russia, and also with Vladivostok State University of Economics and Service, Vladivostok 690014, Russia (e-mail: anton_dys@mail.ru).

O. B. Vitrik is with the Institute of Automation and Control Processes (Far Eastern Branch of Russian Academy of Sciences), Vladivostok 690041, Russia, and also with the Far Eastern Federal University, Vladivostok 690090, Russia (e-mail: oleg_vitrik@mail.ru).

U. A. Eryusheva is with the Far Eastern Federal University, Vladivostok 690090, Russia (e-mail: eriusheva.ua@students.dvfu.ru).

Color versions of one or more of the figures in this paper are available online at http://ieeexplore.ieee.org.

Digital Object Identifier 10.1109/JLT.2018.2871935

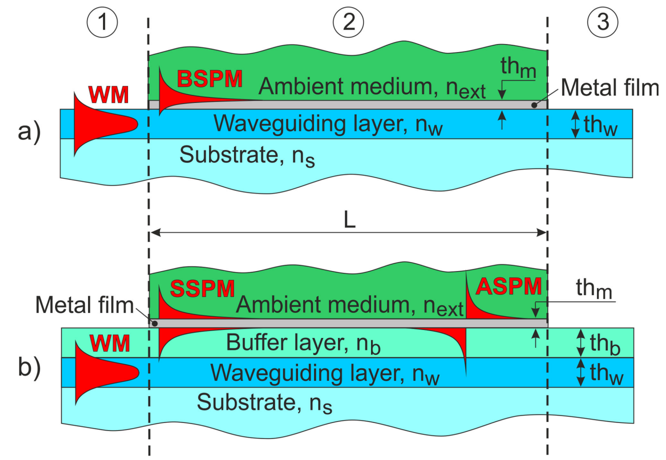

Fig. 1. Schematic representation of the waveguiding structures under study: (a) SPR-refractometer without a buffer layer based on the excitation of bulk surface plasmon mode; (b) SPR-refractometer with buffer layer based on excitation of either symmetric (long-range) or antisymmetric (short-range) surface plasmon modes.

Other authors point out a higher degree of field localization of ASPM, which favors detection of local variations of refractive index in a thin layer near the metal film as well as its very high losses aiding in miniaturization of the SPR-sensor [18], [19]. In [6] a detailed comparison of prism-based configurations using BSPM, SSPM and ASPM is made. However, for waveguide-based SPR-sensors a direct and quantitative comparison, to the best of our knowledge, has not been carried out. The purpose of this paper is thus a comparative analysis of waveguide-based refractometers using bulk, symmetric and antisymmetric surface plasmon modes.

II. Methodology

Schematic diagrams showing BSPM- (a), SSPM- and ASPM-based (b) refractometers under study are presented in Fig. 1. In all three cases the refractometer is made up of three sections: 1, 3 - input and output waveguide sections without metal film, 2 - metallized sensing section. The metal film is in contact with a liquid ambient medium whose refractive index (n_{ext}) is to be measured. We chose silver as a material of the metal film and took its complex-valued permittivity data from handbook [20]. For SPR to be possible the electric field polarization of guided light is assumed to be in the plane of Fig. 1.

The parameters of the waveguiding layer are chosen so as to ensure its single-mode operation. The guided light in Sections 1 and 3 is then described by a single TM fundamental mode. To analyze light propagation in the metallized section two different approaches can be employed. Within the first one, the guided light is considered to be a superposition of two hybrid modes of the multilayer structure of Section 2 viewed as a whole [21]. In the second approach, the metallized section is assumed to support waveguide and surface plasmon modes viewed separately. The interaction between these modes arising when the real parts of their propagation constants are equal or close to one another, as described by the coupled mode theory, leads to the modal amplitudes becoming functions of the distance along the waveguide [21]. This second approach is physically more elucidating and made use of for preliminary analysis and interpretation of numerical results. For numerical modeling, however, it is most convenient to take advantage of the first approach since it is readily available as a standard methodology of modern photonics simulation software, such as Lumerical Mode Solutions used in this work.

To simplify simulation we assumed 2D geometry of the structures under study, which corresponds to an idealized slab waveguide. The obtained results, however, do provide a qualitative understanding of metrological performance of similar 3D structures such as integrated optical refractometers of rectangular cross-section [8], [14], [18], [19] or fiber optic side-polished SPR-probes [7]–[12].

The basic metrological parameter of an SPR-refractometer is its spectral sensitivity [6]:

$$S_{RI} = \frac{d\lambda_{SPR}}{dn_{ext}} = \frac{d\lambda_{SPR}}{dn'_{SP}} \cdot \frac{dn'_{SP}}{dn_{ext}} = S_1\ S_2, \qquad (1)$$

where λ_{SPR} is the central wavelength of the resonant dip in the refractometer's transmission spectrum, n'_{SP} – the real part of surface plasmon mode's effective refractive index, $S_1 = \frac{d\lambda_{SPR}}{dn'_{SP}} = \frac{1}{\frac{dn_{wg}}{d\lambda} - \frac{dn'_{SP}}{d\lambda}}$ - the instrumental sensitivity which depends on the intersection angle of the dispersion curves of the waveguide and surface plasmon modes, λ – wavelength, n_{wg} – effective index of the waveguide mode, S_2 - the physical sensitivity of the surface plasmon mode's effective index to the ambient refractive index.

Apart from spectral sensitivity, SPR-refractometer's resolution is also affected by the width and depth of the resonant dip, noise level in the detection system and other factors [6]. For the sake of comparison of different refractometric configurations, however, it suffices to take into account that resolution is inversely proportional to S_{RI} and the contrast of the resonant dip defined as its depth-to-width ratio [6]. Since attenuation of guided light in a waveguide-based SPR-refractometer can reach several orders of magnitude and its transmission is most conveniently expressed in logarithmic units, it seems reasonable to characterize the width of the dip not by the conventional half-width, but rather by a full width at square root of the minimum (FWSRM) transmission value which corresponds to the half-width of the dip on a logarithmic scale. This width, as calculations show, is larger for higher SPM losses and smaller intersection angle of the dispersion curves of SPM and the waveguide mode.

The depth of the dip depends primarily on the length of the metallized section L. The best resolution is achieved with the deepest resonant dip, but if its depth exceeds the dynamic range of the spectrum analyzer employed, the shape of the dip can be distorted by noise. With this in mind we choose the length of the sensing section, in all cases, so that the attenuation at resonance is ~80 dB, which corresponds roughly to the dynamic range of a modern optical spectrum analyzer (such as Yokogawa AQ6370D).

To compare metrological performance of different refractometric configuration we thus use the so-called Figure-of-Merit (FOM) parameter defined as the ratio of spectral sensitivity to the logarithmic half-width of the resonant dip. Refractometric resolution is inversely proportional to FOM [6] so the best

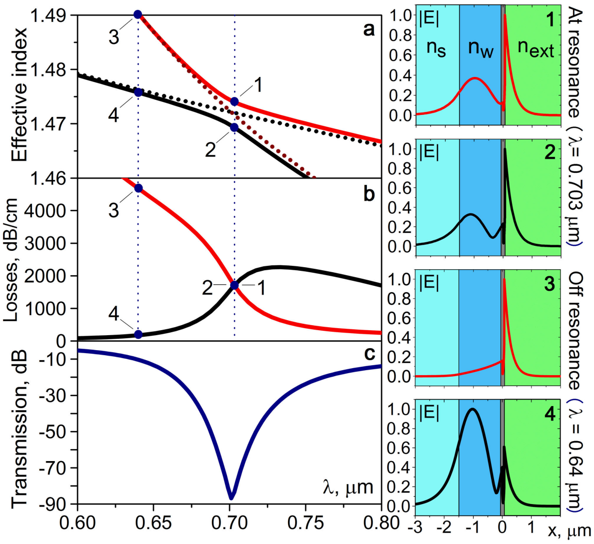

Fig. 2. Spectral dependencies of the effective refractive index (a) and losses (b) of the hybrid modes of the metallized section, as well as the transmission spectrum of the refractometer (c) at $\mathrm{th_m} = 60\,\mathrm{nm}$, $\mathrm{n_{ext}} = 1.4$, $\mathrm{L} = 500\,\mu\mathrm{m}$ .The insets show MMLS profiles at resonance ($\lambda = 0.703\ \mu$m, insets 1, 2) and off resonance ($\lambda = 0.64\ \mu$m, insets 3, 4).

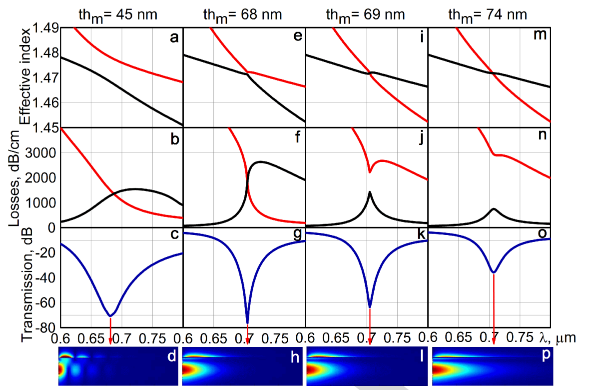

Fig. 3. Effective index and loss spectra of hybrid MMLS, transmission spectra of the refractometer, and electric field amplitude distribution in the metallized section at the resonant wavelength at $\mathrm{n_{ext}} = 1.4$, $\mathrm{L} = 500\,\mu\mathrm{m}$ and $\mathrm{th_m} = 45\,\mathrm{nm}$ (a), (b), (c), (d), 68 nm (e), (f), (g), (h), 69 nm (i), (j), (k), (l), 74 nm (m), (n), (o), (p).

SPR-refractometer with the minimum resolution is the one with the largest FOM value.

Another parameter of an SPR-refractometer, which is important for bio- and chemosensing applications, is the penetration depth ($\mathrm{d_{SP}}$) of the surface plasmon mode into the ambient medium conventionally defined at the 1/e level of the SPM intensity profile. That is because the thickness of the sensing layer of ligand molecules ($\mathrm{d_{lig}}$) can be much smaller than $\mathrm{d_{sp}}$. In this case an SPR-refractometer is more appropriately characterized by the so-called local sensitivity: $S_{loc} \propto S_{RI}\frac{d_{lig}}{d_{SP}}$, which takes proper account of the sensitivity of SPM's propagation constant to refractive index variations in a thin layer near the metal film [6]. It then follows that refractometric resolution with respect to local RI variations should be proportional to the "local resolution coefficient" (LRC) defined as the ratio of $\mathrm{d_{SP}}$ to FOM, which we shall use to compare different SPR-refractometers in terms of local resolution – the smallest LRC value corresponds to the best configuration.

III. Results

A. SPR-Refractometer Without a Buffer Layer

In practical terms it is advantageous to build an SPR-refractometer with the most common and readily available optical materials, so let us choose SiO_2 ($\mathrm{n_s} \sim 1.45$ [20]) as a substrate material and PMMA ($\mathrm{n_w} \sim 1.49$ [22]) as a waveguiding layer material. Numerical calculations then show that for the waveguiding layer thickness $\mathrm{th_w} = 1.5\,\mu\mathrm{m}$ and ambient refractive index $\mathrm{n_{ext}} = 1.4$ the dispersion curves of the separately considered waveguide and bulk surface plasmon modes intersect in the near infrared spectral range (Fig. 2a, dotted lines). By the separately considered BSPM we mean the mode of the metal film localized at metal | ambient medium interface, with the metal film being bounded on one side by the semi-infinite ambient medium and, on the other side, by semi-infinite dielectric with refractive index $\mathrm{n_w}$. By the separately considered waveguide mode (WM) we mean the single fundamental mode of the waveguiding layer bounded by semi-infinite substrate and semi-infinite ambient medium.

According to the coupled mode theory, near the wavelength of intersection of WM and BSPM dispersion curves pronounced losses can occur in Section 2 as a result of transfer of guided light energy to surface plasmons, provided that the WM-BSPM coupling coefficient is sufficiently large. This is indeed the case for the metal film thickness $\mathrm{th_m} = 60\,\mathrm{nm}$, which is confirmed by the results of calculation of the effective index spectra (Fig. 2a, solid lines), loss spectra (Fig. 2b) and profiles (insets 1-4) of the hybrid modes of multilayer structure (MMLS) forming Section 2. It is evident from insets 1 and 2 that at the resonant wavelength MMLS, with their profiles made up of the elements of both BSPM and WM, are indeed a result of the hybridization of the latter modes. Since both MMLS have similar profiles at this wavelength and, therefore, similar overlap integrals with the waveguide mode of Section 1, they are excited at the beginning of Section 2 with about the same amplitudes. Their losses are equally high ($\sim$1700 dB/cm) and result in the attenuation of guided light power by $\sim$80 dB for the length of the metallized section L = 0.5 mm. Off the resonant wavelength, as seen from Fig. 2b and insets 3-4, both profiles and losses of MMLS are quite different. The low loss mode is closer in its profile to the waveguide mode of Section 1 and is, therefore, excited much more efficiently. As a result, there is no significant attenuation of light in Section 2 at this wavelength. It is in this way that a pronounced dip is formed in the transmission spectrum of the refractometer (Fig. 2c).

Numerical calculations show that, depending on the thickness of the metal film, the formation of the resonant dip can occur in two distinct scenarios. If the film thickness is 68 nm or less there is an anticrossing in the effective index spectra of hybrid MMLS, and a crossing in their loss spectra. This is illustrated by Fig. 2a, b ($\mathrm{th_m} = 60\,\mathrm{nm}$) and Fig. 3a, b, e, f ($\mathrm{th_m} = 45; 68\,\mathrm{nm}$). At film thicknesses of 69 nm or more, on the contrary, the MMLS spectra intersect, while their loss spectra do not (Fig. 3i, j, m, n ($\mathrm{th_m} = 69, 74\,\mathrm{nm}$)).

These scenarios can be associated with two different coupling regimes between the separately considered WM and BSPM. The first scenario can be regarded as strong coupling whereby a periodic power exchange takes place at the resonant wavelength between the coupled modes (see also [23] for discussion and [24] for experimental observation of this). This is illustrated by the distribution of the electric field amplitude in Section 2 at a film thickness of 45 nm (Fig. 3d). From the point of view of the entire multilayer structure forming Section 2, this exchange corresponds to interference beats of hybrid MMLS with a period of $\lambda/\Delta n$, where Δn is the difference in their effective indexes at the resonant wavelength. Note that this period increases with increasing film thickness and, for example, at $th_m = 68$ nm, it becomes larger than the characteristic attenuation length of guided light in Section 2. In this case, the exchange of power between WM and BSPM proceeds too slowly to be seen against the background of the overall attenuation of light in Section 2 (Fig. 3h, $th_m = 68$ nm).

The second hybridization scenario can be associated with a weak-coupling regime in which such a periodic power exchange between the waveguide and surface plasmon modes at the resonant wavelength does not occur (see [24] for experimental observation of this regime). In terms of MMLS, this corresponds to a situation where interference beats between them are not possible due to their propagation constants being equal at $\lambda = \lambda_{SPR}$ (Fig. 3i, m).

We must emphasize that the terms "strong" and "weak" coupling are understood here differently than in the context of coupling between lossless modes, and both apply to the resonant wavelength where the real parts of the propagation constants of the coupled modes are exactly equal.

It follows from the coupled mode theory [21] that the coupling regime between WM and BSPM is determined by whether or not the coupling coefficient D is larger than the difference of their effective indexes. At the resonant wavelength the latter reduces, due to WM being lossless, to the imaginary part of the BSPM effective index n''_{SP}. If $D > n''_{SP}$, the dependences of the coupled modes amplitudes on the coordinate along the fiber can be shown to be quasiperiodic, which corresponds to the strong-coupling regime, and for $D < n''_{SP}$ they acquire a quasi-exponential character corresponding to the weak coupling regime.

The coupling coefficient is defined primarily by the thickness of the metal film: for larger th_m the profiles of WM and BSPM overlap less effectively which leads to lower D value and, therefore, weaker coupling. If the coupling becomes too weak ($D << n''_{SP}$), say at $th_m = 74$ nm, the transfer of guided light energy to surface plasmons becomes inefficient which considerably reduces the depth of the resonant dip (Fig. 3o). In terms of MMLS it is explained by the fact that their profiles and losses at the resonant wavelength differ, with lower loss MMLS being closer in its profile to the fundamental mode of Section 1. It is, as a result, excited more effectively and to a greater extent affects the overall transmission of the structure, which leads to the observed reduction of the depth of the dip.

On the other hand, if the coupling is too strong ($D >> n''_{SP}$), for example, at $th_m = 45$ nm, the spectral range around λ_{SPR} where the transfer of energy to surface plasmons is effective gets wider, which leads to the broadening of the resonant dip (Fig. 3c). We thus conclude that the sharpest resonant dip is obtained with the critical coupling - just at the border between weak and strong coupling regimes. At $n_{ext} = 1.4$ this is achieved with a film thickness of 68 nm (Fig. 3g).

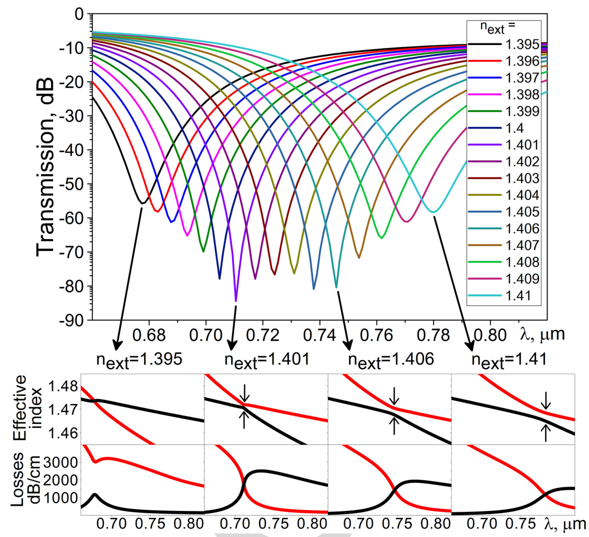

Fig. 4. Calculated transmission spectra of the refractometer for $n_{ext} = 1.395$–1.41, $th_m = 68$ nm, L = 0.5 mm. Shown in the insets below are the effective index and loss spectra of MMLS of Section 2 at $n_{ext} = 1.395$; 1.401; 1.406; 1.41.

The ambient refractive index, however, does not remain constant in the course of refractometric measurements. Its variation shifts the resonant wavelength, which, for a fixed value of th_m, is inevitably accompanied by changes in the resonant dip contrast. This is illustrated in Fig. 4 depicting transmission spectra of the refractometer calculated for $th_m = 68$ nm, $n_{ext} = 1.395$–1.41, L = 0.5 mm. As evident from the dispersion curves of hybrid MMLS shown in the insets at the bottom of Fig. 4 the coupling between WM and BSPM gets stronger with increasing n_{ext} and λ_{SPR}. This is explained by the fact that, firstly, the profiles of WM and BSPM broaden as the wavelength increases and overlap more effectively thus leading to a larger coupling coefficient. Secondly, n''_{SP} value responsible for the losses of BSPM tend to decrease with increasing wavelength [6], which also makes the coupling stronger.

Thus the depth of the resonant dip first gradually growths while shifting from left to right with increasing n_{ext} as the coupling gets stronger but is still in the weak coupling regime ($n_{ext} < 1.4$). The switching to the strong coupling regime occurs at $n_{ext} \sim 1.4$ after which the coupling continues to grow stronger as seen from the growing difference in the effective indexes of MMLS at the resonant wavelength (marked with arrows in the insets of Fig. 4). At $n_{ext} > 1.4$ one can also observe slight quasiperiodic variations in the depth of the resonant dip. They arise from the periodic power exchange between the waveguide and surface plasmon modes resulting into the guided light, depending on the period of the exchange, being predominantly localized at the end of Section 2 either in the region of the waveguiding layer or near the metal film. This affects the transmission loss between Sections 2 and 3, which varies as the

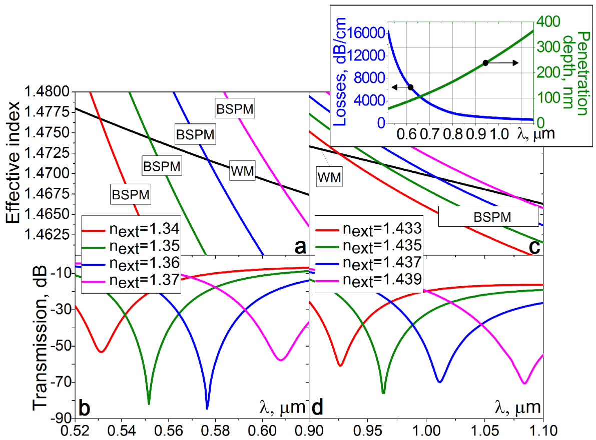

Fig. 5. Effective index spectra for the separately considered waveguide and bulk surface plasmon modes as well as transmission spectra of the refractometer at $th_m = 58$ nm, $th_w = 1\ \mu$m, L = 0.2 mm, $n_{ext} = 1.34$–1.37 (a), (b) and at $th_m = 75$ nm, $th_w = 2.5\ \mu$m, L = 1.3 mm, $n_{ext} = 1.433$–1.439 (c), (d). The upper-right inset shows the spectral dependences of losses and depth of penetration of BSPM into the ambient medium.

period of the exchange gets shorter with stronger coupling, thus leading to the observed variations in the depth of the dip.

When the ambient refractive index exceeds ∼1.406 the resonant dip broadens due to WM-BSPM coupling becoming overly strong and its depth decreases due to lower losses of BSPM at longer wavelengths.

It then seems reasonable to define a range of efficient refractometric measurements (Δn_{ext}) as the range of n_{ext} values for which the depth of the resonant dip is less than the maximum depth by not more than an arbitrary threshold value, say 20 dB. For the configuration under study, as seen from Fig. 4, this corresponds roughly to n_{ext} ranging from 1.395 to 1.41, i.e., $\Delta n_{ext} \cong 0.015$. It also follows from the analysis of the transmission spectra in Fig. 4 that the spectral sensitivity of the refractometer is $S_{RI} \cong 6800$ nm/ RI unit (RIU), logarithmic half-width of the dip in the middle of the measured n_{ext} range – FWSRM ≅ 25 nm. The penetration depth of BSPM into the ambient medium at $\lambda \sim 700$ nm is $d_{sp} \cong 120$ nm (see the inset of Fig. 5), which yields FOM ≅ 270 and LRC ≅ 0.44.

It should be noted that the SPR-refractometer under consideration can be used for measuring other values of ambient refractive index, both higher and lower than 1.4. For example, at $n_{ext} \sim 1.35$ the phase-matching condition between the waveguide and surface plasmon modes is fulfilled near $\lambda = 550$ nm (Fig. 5a). The optimal film thickness in this case is 58 nm. For the waveguide layer to remain in the single-mode regime its width is reduced to 1 micron. Since the losses of BSPM in this spectral range are several times higher than those at $\lambda \sim 700$ nm (inset of Fig. 5) we also reduce the length of the metallized section to 0.2 mm.

In spite of the higher losses of BSPM the width of the resonant dip turns out in this case to be less than in the previous one: FWSRM ≅ 16 nm (at $n_{ext} \cong 1.35$), which can be explained by a much larger angle of intersection of WM and BSPM dispersion curves (Fig. 5a). It is for the same reason that, although physical sensitivity of BSPM's effective index to the ambient RI is larger at shorter wavelengths [6], the overall spectral sensitivity turns out in this case to be about 2.5 times lower than that at $\lambda \sim 700$ nm: $S_{RI} \cong 2600$ nm/RIU due to a drop in the instrumental sensitivity. The rage of measured refractive index is correspondingly larger: $\Delta n_{ext} \cong 0.03$. FOM amounts to ∼162 which is more than 1.5 times worse than in the previous case. The penetration depth of BSPM into the ambient medium, however, at $\lambda \sim 550$ nm is only ∼70 nm (inset of Fig. 5), so in terms of the local resolution there is virtually no difference from the previous case: LRC ≅ 0.43.

At a higher value of the ambient refractive index: $n_{ext} \sim 1.435$ the phase-matching condition between the waveguide and surface plasmon modes is fulfilled at $\lambda \sim 1000$ nm (Fig. 5c). The optimal waveguide width and metal film thickness in this case are 2.5 μm and 75 nm, respectively. The losses of BSPM in this spectral range are much lower than at $\lambda \sim 700$ nm or $\lambda \sim 550$ nm, so to get a ∼80 dB resonant dip the length of the metallized section has to be extended to L = 1.3 mm. Secondly, the dispersion curves of WM and BSPM intersect here at a much smaller angle than in both cases considered above. This leads to a much higher spectral sensitivity due to a larger instrumental contribution: $S_{RI} \cong 26000$ nm/ RIU, narrowing of the measured RI range: $\Delta n_{ext} \cong 0{,}008$, and broadening of the resonant dip. The latter feature is, however, partially compensated by the lower losses of BSPM in this spectral range resulting in FWSRM ≅ 44 nm (at $n_{ext} \cong 1.435$). There is thus a significant advantage in terms combination of spectral sensitivity and width of the dip as compared to the previous cases: FOM ≅ 590. The local resolution is, however, virtually unchanged because of much deeper penetration of BSPM into the ambient medium at $\lambda \sim 1000$ nm ($d_{SP} \cong 270$ nm, inset of Fig. 5): LRC ≅ 0.46.

B. SPR-Refractometer Based on Symmetric (Long-Range) Surface Plasmon Mode

Introduction of a buffer layer between the waveguide and metal film with the refractive index close to that of the ambient medium enables one to build an SPR-refractometer both on symmetric (long-range) and antisymmetric (short-range) surface plasmon modes [6]. SSPM and ASPM differ significantly in their properties both from each other and from the bulk surface plasmon mode considered above. The metrological parameters of corresponding SPR-refractometers can, therefore, be widely different as well. To gain a benefit in metrological performance one must to the fullest possible extent exploit the advantages that a particular plasmon mode has to offer in terms of building an SPR-refractometer.

As for the long-range surface plasmon mode its major strength is in its low propagation losses [6], [15]–[17]. This enables one to obtain a reasonably narrow resonant dip even with a very small intersection angle between WM and SSPM dispersion curves, which may yield a very high spectral sensitivity due to a large instrumental contribution. The losses of SSPM tend to decrease for larger wavelength and thinner metal film [6], which makes it reasonable to use a long-wavelength spectral range and a thin metal film. Making the film too thin, however, is not practical and can be technologically challenging. At too long a wavelength, on the other hand, the intersection angle can become too small to produce a distinct resonant dip

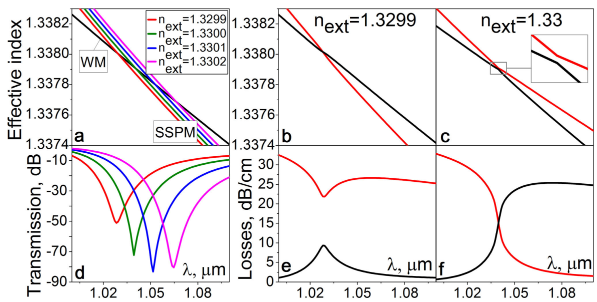

Fig. 6. Dispersion curves of the separately considered waveguide and symmetric surface plasmon modes (a) and transmission spectra of the SSPM-based refractometer (d) for $n_{ext} = 1.3299$–1.3302; effective index and loss spectra of the hybrid MMLS of the metallized section for $n_{ext} = 1.3299$ (b), (e) and 1.33 (c), (f) (L = 60 mm, $th_w = 200$ nm, $th_b = 13.3\ \mu$m, $th_m = 20$ nm).

in spite of SSPM's low losses. With thus choose as a compromise $th_m = 20$ nm and $\lambda \sim 1000$ nm. We note also that the effective index of the long-range surface plasmon mode is much lower than those of ASPM and BSPM, so to phase-match it to the waveguide mode one has to use materials with low optical density. The specified requirements are fulfilled e.g., with the following waveguiding structure: substrate made of Cytop polymer ($n_s \sim 1.34$ [25]), waveguiding layer – MgF_2 ($n_w \sim 1.37$ [26], $th_w = 200$ nm), buffer layer – Cytop, silver film ($th_m = 20$ nm).

Fig. 6a shows the dispersion curves of the separately considered WM and SSPM calculated for the chosen structure at $n_{ext} = 1.33$. As seen from the figure the phase-matching between the two modes can be achieved near $\lambda = 1040$ nm. To ensure the maximum contrast of the resonant dip we also require the switching from the weak to strong regime of WM-SSPM coupling to occur around this wavelength. Unlike the previously considered configuration, in the SPR-refractometer with a buffer layer it is the thickness of the buffer layer that is primarily responsible for the coupling regime. Calculation show that the optimal value of th_b at which the switching of coupling regimes occurs near $\lambda = 1040$ at $n_{ext} \cong 1.33$ amounts to 13.3 microns (Fig. 6b, c, e, f).

The transmission spectra of the refractometer calculated for $n_{ext} = 1.3299$–1.3302, $th_b = 13.3\ \mu$m are shown in Fig. 6d. One can conclude from the figure that spectral sensitivity in this case amounts to as high as ~120000 nm/RIU, $\Delta n_{ext} \cong 0{,}0004$, FWSRM $\cong$ 18 nm (at $n_{ext} \cong 1.3301$), i.e., FOM $\cong$ 6670, which is more than an order of magnitude higher than that of the SPR-refractometer without a buffer layer. In spite of the penetration depth of SSPM into the ambient medium being much higher than that of BSPM ($d_{SP} \cong 580$ nm at $\lambda \sim 1050$ nm) in terms of local resolution the SPR-refractometer based on SSPM has a significant advantage as well: LRC $\cong$ 0.09 which is ~5 times below that of SPR-refractometer without a buffer layer. We must note, however, that the advantage in metrological performance arises from the low losses of SSPM (~30 dB/cm at $\lambda \sim 1050$ nm) and it comes, therefore, at a cost of extending the length of the sensing section: an ~80dB resonant dip is achieved with the sensing section being as long as 6 cm.

If needed the sensing section can be shortened by choosing the parameters of the structure so that the SPR condition is fulfilled at a shorter wavelength where SSPM has higher losses. For example, at $th_w = 400$ nm and $n_{ext} = 1.33$ the waveguide mode is phase-matched to SSPM at around $\lambda = 600$ nm. The optimal thickness of the buffer layer is $th_b = 2.6\ \mu$m. The losses of SSPM in this spectral range are about an order of magnitude higher than those at $\lambda \sim 1000$ nm: ~310 dB/cm enabling 10-fold shortening of the sensing section: L = 6 mm. The spectral sensitivity, however, turns out in this case to be only about a tenth of that at $\lambda \sim 1000$ nm due to a sharp drop in the instrumental contribution: $S_{RI} \cong 16000$ nm/ RIU, which is accompanied by broadening of the RI measurement range: $\Delta n_{ext} \cong 0.003$ and some narrowing of the resonant dip: FWSRM $\cong$ 12 nm. Thus, in terms of combination of sensitivity and resonant dip width such a configuration is more than 5 times inferior to the previous one: FOM $\cong$ 1330. The local resolution is, however, not much worse than that in the previous case due to much a lower penetration depth of SSPM at $\lambda \sim 600$ nm than at $\lambda \sim 1000$ nm ($d_{sp} \cong 200$ nm): LRC $\cong$ 0.15.

C. SPR-Refractometer Based on the Antisymmetric (Short-Range) Surface Plasmon Mode

From the analysis of the properties of the antisymmetric surface plasmon mode [6] one can conclude that its main advantages in terms of building an SPR refractometer are as follows. Firstly, it has a higher degree of field localization near the film which may lead to better sensitivity to local variations of refractive index. Secondly, it has a higher physical sensitivity to the ambient refractive index as compared to SSPM. Thirdly, higher losses of ASPM allow one to obtain a deep resonant dip with a very short sensing section, which aids in miniaturization of the refractometer. All of these features become more pronounced with decreasing wavelength and metal film thickness [6]. Another circumstance to take into account is that, as calculations show, when the media on two sides of the film differ in refractive indexes the profile of ASPM tends to shift to the optically denser medium, which brings about additional increase in sensitivity to the refractive index of that medium. Thus in order to exploit ASPM's advantages to the fullest degree one should use shorter wavelength range, very thin film and make the refractive index of the buffer layer somewhat lower than that of the ambient medium. Due to the effective index of ASPM being quite high [6], to enable its phase-matching with the waveguide mode one should use for the waveguiding layer a high optical density material.

The stated requirements are satisfied e.g., with the following structure: substrate – SiO_2, waveguiding layer – Si_3N_4 ($n_w \sim 2$ [27], $th_w = 250$ nm), buffer layer – Teflon AF2400 ($n_b \sim 1.28$ [28]), silver film ($th_m = 20$ nm), ambient medium ($n_{ext} > n_b$).

Fig. 7a shows the dispersion curves of the separately considered waveguide and antisymmetric plasmon modes calculated for the chosen structure at different n_{ext} values in the range 1.34–1.37. As one can see, the SPR condition is fulfilled at $\lambda \sim 640$ nm where ASPM losses are found to be as high as ~42000 dB/cm. The optimal thickness of the buffer layer at which the switching of WM-ASPM coupling regimes occurs near this wavelength is $th_b = 180$ nm (Fig. 7b, c, e, f). The losses of hybrid MMLS at the resonant wavelength reach

TABLE I
SPECIFICATIONS OF THE SPR-REFRACTOMETERS UNDER STUDY

	SPR-refractometer without a buffer layer			SPR-refractometer based on long-range surface plasmon mode		SPR-refractometer based on short-range surface plasmon mode	
Measured RI, $\overline{n_{ext}} \pm \frac{\Delta n_{ext}}{2}$	1.355±0.015	1.404±0.0075	1.437±0.004	1.33±0.0015	1.3301±0.0002	1.355±0.015	1.33±0.01
Resonant wavelength range, nm	530-610	680-780	920-1120	600-650	1030-1080	625-655	900-980
Instrumental sensitivity, S_1	2 000	6 000	24 000	34 000	316 000	825	4 350
Physical sensitivity, S_2	1.26	1.14	1.08	0.47	0.38	1.09	0.85
Spectral sensitivity S_{RI}, nm/RIU	**2 600**	**6 800**	**26 000**	**16 000**	**120 000**	**900**	**3 700**
FWSRM, nm	**16**	**25**	**44**	**12**	**18**	**35**	**65**
FOM	**162**	**270**	**590**	**1 330**	**6 670**	**25,7**	**57**
SPM losses near λ_{SPR}, dB/cm	11 620	3 650	970	310	30	42 000	11 000
Length of the sensing section, mm	**0.2**	**0.5**	**1.3**	**6**	**60**	**0.04**	**0.18**
SPM penetration, d_{SP}, nm	70	120	270	200	580	44	117
Local resolution coefficient, LRC	**0.43**	**0.44**	**0.46**	**0.15**	**0.09**	**1.7**	**2.05**

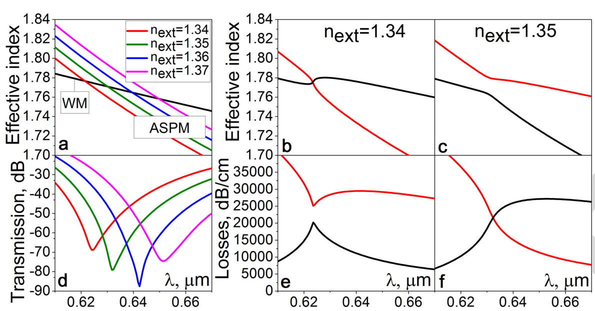

Fig. 7. Dispersion curves of the separately considered waveguide and antisymmetric surface plasmon modes (a), as well as transmission spectra of the ASPM-based refractometer (d) calculated for $n_{ext} = 1.34$–1.37; effective index and loss spectra of hybrid MMLS of the metallized section calculated for $n_{ext} = 1.37$ (b), (e) and 1.35 (c), (f) ($L = 0.04$ mm, $th_w = 250$ nm, $th_b = 180$ nm, $th_m = 20$ nm).

~22 000 dB/cm which makes it possible to reduce the length of the sensing section to just $L = 40$ μm.

The transmission spectra of the refractometer are shown in Fig. 7d. It can be concluded from the figure that the spectral sensitivity is in this case ~900 nm/RIU, $\Delta n_{ext} \cong 0.03$, FWSRM $\cong$ 35 nm (at $n_{ext} \cong 1.36$), and FOM $\cong$ 25.7, which is about an order of magnitude lower than the FOM of the refractometer without a buffer layer and 260 times lower than the FOM of the refractometer on SSPM. The penetration depth of ASPM into the ambient medium, however, at $\lambda \sim 640$ nm is just ~44 nm and LRC amounts, therefore, to ~1.7.

We note that such a low sensitivity results from an extraordinarily low instrumental contribution due to a very large intersection angle of WM and ASPM dispersion curves. The parameters of the waveguiding structure can be adjusted to shift the resonance to a longer wavelength thus decreasing the intersection angle and enhancing the sensitivity. This will also broaden the resonant dip but due to ASPM losses falling with wavelength some benefit should be expected in terms of FOM parameter (at the expense of a longer sensing section). For example, at $th_b = 150$ nm and $n_{ext} \sim 1.33$ the SPR condition is fulfilled at $\lambda \sim 900$ nm where the losses of ASPM amount to ~11000 dB/cm. At the optimal film thickness ($th_b = 568$ nm) an 80-dB resonant dip can be obtained with a sensing section of 180 μm. The spectral sensitivity is then found to be ~3700 nm/RIU, $\Delta n_{ext} \cong 0.02$, FWSRM $\cong$ 65 nm, $d_{SP} \cong 117$ nm, which results in FOM $\cong$ 57 and LRC $\cong$ 2.05.

IV. DISCUSSION

The specifications of the studied BSPM, SSPM- and ASPM-based refractometers are summarized in Table I. As seen from the table the difference in metrological performance of different configurations results mainly from their spectral sensitivity. The physical sensitivity, however, does not change much and the observed variations are primarily due to the greatly varying instrumental contribution.

The best specifications are achieved with the SPR-refractometer based on symmetric or long-range surface plasmon mode: due to its low losses a sharp resonant dip can be obtained even with a very small intersection angle of WM and SSPM dispersion curves yielding an extremely high instrumental and hence overall spectral sensitivity. The advantage in terms of FOM parameter reaches about two orders of magnitude as compared to the ASPM-based SPR-refractometer and one order of magnitude as compared to the SPR-refractometer without a buffer layer.

Apart from its low losses the symmetric surface plasmon mode has a larger penetration depth into the ambient medium. In terms of local resolution, therefore, the advantage of using SSPM instead of ASPM or BSPM is less pronounced: LRC is about 20 times lower than that for ASPM and ~6 times lower than that for BSPM.

We should also emphasize that the advantage in metrological performance of the SPR-refractometer based on symmetric surface plasmon mode comes at a cost of extending the length of the metallized section: to obtain a resonant dip of the same depth as in ASPM- and BSPM-based refractometers a much longer (up to three orders of magnitude) sensing section is required.

The most compact sensing element with the minimum length of the sensing section is characteristic of the SPR-refractometer based on the antisymmetric surface plasmon mode. It has, however, the worst metrological performance among all the studied configurations due to the enormous losses of ASPM.

The SPR-refractometer without a buffer layer occupies an intermediate position between those based on SSPM and ASPM, both in terms of metrological performance and sensing section length. It has, however, an important practical advantage of having the simplest structure, which facilitates the fabrication process.

One can also conclude from the table that the values of measured refractive index depend both on the parameters of the metallized section and on the working spectral range. By choosing a longer wavelength range where a surface plasmon mode has lower losses (and using a longer sensing section) one can obtain higher metrological performance in terms of FOM parameter. The local resolution coefficient, however, does not change much since the increase in FOM is offset by a higher penetration depth of SPM into the ambient medium. We also note that if the resonant wavelength is shifted too far into the infrared ($\lambda_{SPR} \gtrsim$ 1200 nm) the intersection angle between WM and SPM dispersion curves may get so small that refractometric measurements, in spite of a very high sensitivity, become no longer possible due to smearing out of the resonant dip.

In closing, we emphasize that metrological parameters summarized in Table I have been obtained in the 2D-geometry approximation and depend on the specific choices of materials and geometric parameters of the refractometers. Their primary purpose is, therefore, not to characterize performance of practical SPR-sensors but to illustrate in a quantitative manner the relative merits of refractometers based on bulk, symmetric and antisymmetric surface plasmon modes. The revealed patterns and relationships, we believe, are also valid in 3D geometry and do not depend on the specific details of the refractometers.

V. Conclusions

We have thus studied three SPR-refractometer configurations: without a buffer layer based on the excitation of the bulk surface plasmon mode, and with a buffer layer using symmetric (long-range) and antisymmetric (short-range) surface plasmon modes. It is shown the highest metrological performance is achieved with the symmetric SPM, which, however, requires a much longer sensing section. If miniaturization of the sensor is of utmost importance the preferred type of plasmon mode to use is the antisymmetric one, which enables minimization of the sensing section length at a cost of impaired metrological specifications. Finally, in terms of ease of fabrication the most attractive configuration is that without a buffer layer, which is intermediate between SSPM- and ASPM-based refractometers both in terms of metrological performance and sensing section length.

References

[1] A. Rasooly and K. E. Herold, *Biosensors and Biodetection*. New York, NY, USA: Humana, 2009.

[2] Ligler F. S. and C. R. Taitt, *Optical Biosensors: Today and Tomorrow*. Amsterdam, The Netherlands: Elsevier, 2011.

[3] F. Baldini *et al.*, *Optical Chemical Sensors*. Berlin, Germany: Springer Science & Business Media, 2006, vol. 224.

[4] X. Guo and J. Biophoton,"Surface plasmon resonance based biosensor technique: A review," *J. Biophoton.*, vol. 5, pp. 483–501, 2012.

[5] J. Homola, "Surface plasmon resonance sensors for detection of chemical and biological species," *Chem. Rev.*, vol. 108, no. 2, pp. 462–493, 2008.

[6] J. Homola, *Surface Plasmon Resonance Based Sensors*. Berlin, Germany: Springer-Verlag, 2006.

[7] B. D. Gupta and R. K. Verma "Surface plasmon resonance-based fiber optic sensors: Principle, probe designs, and some applications," *J. Sensors*, vol. 2009, 2009, Art. no. 979761.

[8] R. Kashyap and G. Nemova, "Surface plasmon resonance-based fiber and planar waveguide sensors," *J. Sensors*, vol. 2009, 2009, Art. no. 645162.

[9] C. Caucheteur, T. Guo, and J. Albert "Review of plasmonic fiber optic biochemical sensors: Improving the limit of detection," *Analytical Bioanalytical Chem.*, vol. 407, no. 14, pp. 3883–3897, 2015.

[10] E. Klantsataya *et al.*, "Plasmonic fiber optic refractometric sensors: From conventional architectures to recent design trends," *Sensors*, vol. 17, no. 1, 2016, Art. no. 12.

[11] S. K. Srivastava and B. D. Gupta, "Fiber optic plasmonic sensors: Past, present and future," *Open Optics J.*, vol. 7, no. 1, pp. 58–83, 2013.

[12] M. E. Bosch *et al.*, "Recent development in optical fiber biosensors," *Sensors*, vol. 7, no. 6, pp. 797–859, 2007.

[13] A. V. Dyshlyuk *et al.*, "Numerical and experimental investigation of surface plasmon resonance excitation using whispering gallery modes in bent metal-clad single-mode optical fiber," *J. Lightw. Technol.*, vol. 35, no. 24, pp. 5425–5431, Dec. 2017.

[14] Y.-S. Chu *et al.*, "Surface plasmon resonance sensors using silica-on-silicon optical waveguides," *Microw. Opt. Technol. Lett.*, vol. 48, no. 5, pp. 955–957, 2006.

[15] G. G. Nenninger *et al.*, "Long-range surface plasmons for high-resolution surface plasmon resonance sensors," *Sensors Actuators B: Chem.*, vol. 74, no. 1–3, pp. 145–151, 2001.

[16] R. Slavík and J. Homola, "Ultrahigh resolution long range surface plasmon-based sensor," *Sensors Actuators B: Chem.*, vol. 123, no. 1, pp. 10–12, 2007.

[17] J. Dostálek, A. Kasry, and W. Knoll, "Long range surface plasmons for observation of biomolecular binding events at metallic surfaces," *Plasmonics*, vol. 2, no. 3, pp. 97–106, 2007.

[18] B. Fan, F. Liu, Y. Li, Y. Huang, Y. Miura, and D. Ohnishi, "Refractive index sensor based on hybrid coupler with short-range surface plasmon polariton and dielectric waveguide," *Appl. Phys. Lett.*, vol. 100, no. 11, 2012, Art. no. 111108.

[19] B. Fan *et al.*, "Integrated refractive index sensor based on hybrid coupler with short range surface plasmon polariton and dielectric waveguide," *Sensors Actuators B: Chem.*, vol. 186, pp. 495–505, 2013.

[20] E. D. Palik *Handbook of Optical Constants of Solids*. New York, NY, USA: Academic, 1998.

[21] A. W. Snyder and J. Love *Optical Waveguide Theory*. Berlin, Germany: Springer Science & Business Media, 2012.

[22] N. Sultanova, S. Kasarova, and I. Nikolov, "Dispersion properties of optical polymers," *Acta Physica Polonica-Series A Gen. Phys.*, vol. 116, no. 4, pp. 585–587, 2009.

[23] M. L. Nesterov, A. V. Kats, and S. K. Turitsyn, "Extremely short-length surface plasmon resonance devices," *Optics Express* vol. 16, no. 25, pp. 20227–20240, 2008.

[24] H. Ditlbacher *et al.*, "Coupling dielectric waveguide modes to surface plasmon polaritons," *Opt. Express*, vol. 16, no. 14, pp. 10455–10464, 2008.

[25] 2018. [Online]. Available: http://www.bellexinternational.com/products/cytop/pdf/cytop-catalog.pdf

[26] H. H. Li, "Refractive index of alkaline earth halides and its wavelength and temperature derivatives," *J. Phys. Chem. Ref. Data*, vol. 9, no. 1, pp. 161–290, 1980.

[27] H. R. Philipp, "Optical properties of silicon nitride," *J. Electrochemical Soc.*, vol. 120, no. 2, pp. 295–300, 1973.

[28] M. K. Yang, R. H. French, and E. W. Tokarsky, "Optical properties of Teflon AF amorphous fluoropolymers," *J. Micro/Nanolithography, MEMS, MOEMS*, vol. 7, no. 3, 2008, Art. no. 033010.

Authors' biographies not available at the time of publication.

Waveguide-Based Refractometers Using Bulk, Long-and Short-Range Surface Plasmon Modes: Comparative Study

Anton V. Dyshlyuk, Oleg B. Vitrik, and Uliana A. Eryusheva

***Abstract*—We present a numerical study comparing three configurations of the waveguide-based surface plasmon resonance refractometer: without a buffer layer based on the excitation of the bulk surface plasmon mode, and with a buffer layer using the symmetric (long-range) and antisymmetric (short-range) plasmon modes. Optimal conditions ensuring the sharpest resonant dip in the refractometer's transmission spectrum are identified. Relative merits of various configurations in terms of the figure-of-merit parameter, local sensitivity to refractive index variations near the metal film, and the size of the sensing element are quantified and discussed.**

***Index Terms*—Biosensing, chemosensing, long-range surface plasmon mode, short-range surface plasmon mode, SPR, surface plasmon resonance, waveguide-based SPR-refractometer.**

I. Introduction

REFRACTOMETRIC sensors based on surface plasmon resonance (SPR) represent a topical trend in modern bio- and chemosensing technologies [1]–[4]. Sensors of this kind use resonant excitation of surface plasmon waves (coupled oscillations of free electron density and electromagnetic field bound to a metal-dielectric interface) to detect minute variations in refractive index induced by (bio)chemical reactions near the interface [4]–[6].

The most common configuration of the SPR-refractometer is the well-known Kretschmann scheme, in which surface plasmons are excited by a beam of light incident from within a prism on its metal-coated facet [4]–[6]. This configuration is widely used in laboratory-based biochemical researches, but it is not suited for making portable and inexpensive sensors, including disposable and point-of-care devices. Considerable research efforts, therefore, are devoted to the development of waveguide-based SPR-refractometers in which a surface plasmon mode (SPM) is excited by modes of a dielectric waveguide [5]–[14], [18], [19]. Sensors of this type, in contrast to the Kretschmann configuration, can be easily miniaturized and coupled to fiber and integrated optics elements, can be used for measurements in situ and in hard-to-reach locations, as well as aid in cost reduction of SPR bio- and chemosensing systems [7]–[11].

Among various types of waveguide-based SPR-refractometers known to date the simplest one is probably the waveguide analog of the Kretschmann scheme, in which a metal film is deposited directly onto the light-guiding core of a waveguide [5]–[8], [10], [14]. Other configurations have also been proposed, which use a buffer layer between the core and the metal film with the refractive index close to that of the ambient medium [8]–[10], [15]–[19]. In the latter case it is possible to make use of either symmetric (long-range) or antisymmetric (short-range) surface plasmon modes arising due to the hybridization of surface plasmon modes supported by different sides of a thin metal film [5], [6].

We should note that in the SPR-refractometer without a buffer layer, similarly to the Kretschmann scheme, the refractive index of the waveguiding layer is typically much larger than that of the ambient medium. This makes the propagation constants of the surface plasmon modes at two sides of the metal film quite different so that they cannot hybridize effectively even if the film is very thin. Hence, the plasmon mode excited in the SPR-refractometer without a buffer layer is localized at the metal | ambient medium interface and is very close in its characteristics to the SPM at the surface of a bulk metal. We shall thus refer to it as the 'bulk surface plasmon mode' (BSPM) as opposed to the symmetric surface plasmon mode (SSPM) and antisymmetric surface plasmon mode (ASPM) in the refractometer with a buffer layer.

Symmetric, antisymmetric and bulk plasmon modes differ in their propagation constants, losses, penetration depths and sensitivity to the ambient refractive index [6]. As to which of the modes is most suitable for building an SPR-refractometer there seems to be no apparent consensus in the published literature. Those authors who propose refractometers based on SSPM emphasize its lower losses and, correspondingly, a narrower resonant dip in the transmission spectrum as well as higher spectral sensitivity [15]–[17].

Manuscript received May 30, 2018; revised August 9, 2018; accepted September 2, 2018. The work was supported by the Russian Science Foundation under Grant 16-12-10165. *(Corresponding author: Anton V. Dyshlyuk.)*

A. V. Dyshlyuk is with the Far Eastern Federal University, Vladivostok 690090, Russia, and also with Vladivostok State University of Economics and Service, Vladivostok 690014, Russia (e-mail: anton_dys@mail.ru).

O. B. Vitrik is with the Institute of Automation and Control Processes (Far Eastern Branch of Russian Academy of Sciences), Vladivostok 690041, Russia, and also with the Far Eastern Federal University, Vladivostok 690090, Russia (e-mail: oleg_vitrik@mail.ru).

U. A. Eryusheva is with the Far Eastern Federal University, Vladivostok 690090, Russia (e-mail: eriusheva.ua@students.dvfu.ru).

Color versions of one or more of the figures in this paper are available online at http://ieeexplore.ieee.org.

Digital Object Identifier 10.1109/JLT.2018.2871935

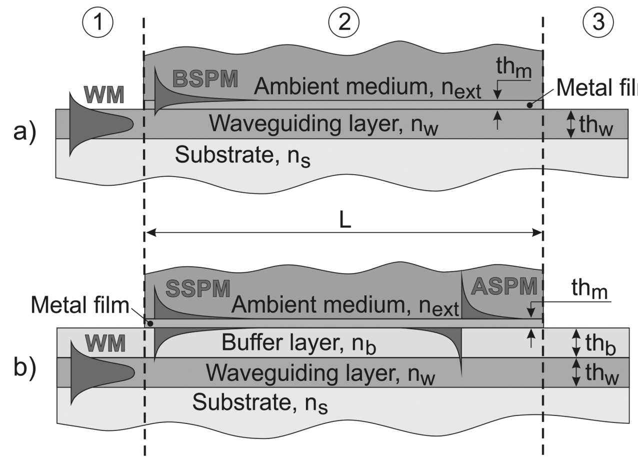

Fig. 1. Schematic representation of the waveguiding structures under study: (a) SPR-refractometer without a buffer layer based on the excitation of bulk surface plasmon mode; (b) SPR-refractometer with buffer layer based on excitation of either symmetric (long-range) or antisymmetric (short-range) surface plasmon modes.

Other authors point out a higher degree of field localization of ASPM, which favors detection of local variations of refractive index in a thin layer near the metal film as well as its very high losses aiding in miniaturization of the SPR-sensor [18], [19]. In [6] a detailed comparison of prism-based configurations using BSPM, SSPM and ASPM is made. However, for waveguide-based SPR-sensors a direct and quantitative comparison, to the best of our knowledge, has not been carried out. The purpose of this paper is thus a comparative analysis of waveguide-based refractometers using bulk, symmetric and antisymmetric surface plasmon modes.

II. Methodology

Schematic diagrams showing BSPM- (a), SSPM- and ASPM-based (b) refractometers under study are presented in Fig. 1. In all three cases the refractometer is made up of three sections: 1, 3 - input and output waveguide sections without metal film, 2 - metallized sensing section. The metal film is in contact with a liquid ambient medium whose refractive index (n_{ext}) is to be measured. We chose silver as a material of the metal film and took its complex-valued permittivity data from handbook [20]. For SPR to be possible the electric field polarization of guided light is assumed to be in the plane of Fig. 1.

The parameters of the waveguiding layer are chosen so as to ensure its single-mode operation. The guided light in Sections 1 and 3 is then described by a single TM fundamental mode. To analyze light propagation in the metallized section two different approaches can be employed. Within the first one, the guided light is considered to be a superposition of two hybrid modes of the multilayer structure of Section 2 viewed as a whole [21]. In the second approach, the metallized section is assumed to support waveguide and surface plasmon modes viewed separately. The interaction between these modes arising when the real parts of their propagation constants are equal or close to one another, as described by the coupled mode theory, leads to the modal amplitudes becoming functions of the distance along the waveguide [21]. This second approach is physically more elucidating and made use of for preliminary analysis and interpretation of numerical results. For numerical modeling, however, it is most convenient to take advantage of the first approach since it is readily available as a standard methodology of modern photonics simulation software, such as Lumerical Mode Solutions used in this work.

To simplify simulation we assumed 2D geometry of the structures under study, which corresponds to an idealized slab waveguide. The obtained results, however, do provide a qualitative understanding of metrological performance of similar 3D structures such as integrated optical refractometers of rectangular cross-section [8], [14], [18], [19] or fiber optic side-polished SPR-probes [7]–[12].

The basic metrological parameter of an SPR-refractometer is its spectral sensitivity [6]:

$$S_{RI} = \frac{d\lambda_{SPR}}{dn_{ext}} = \frac{d\lambda_{SPR}}{dn'_{SP}} \cdot \frac{dn'_{SP}}{dn_{ext}} = S_1\ S_2, \qquad (1)$$

where λ_{SPR} is the central wavelength of the resonant dip in the refractometer's transmission spectrum, n'_{SP} – the real part of surface plasmon mode's effective refractive index, $S_1 = \frac{d\lambda_{SPR}}{dn'_{SP}} = \frac{1}{\frac{dn_{wg}}{d\lambda} - \frac{dn'_{SP}}{d\lambda}}$ - the instrumental sensitivity which depends on the intersection angle of the dispersion curves of the waveguide and surface plasmon modes, λ – wavelength, n_{wg} – effective index of the waveguide mode, S_2 - the physical sensitivity of the surface plasmon mode's effective index to the ambient refractive index.

Apart from spectral sensitivity, SPR-refractometer's resolution is also affected by the width and depth of the resonant dip, noise level in the detection system and other factors [6]. For the sake of comparison of different refractometric configurations, however, it suffices to take into account that resolution is inversely proportional to S_{RI} and the contrast of the resonant dip defined as its depth-to-width ratio [6]. Since attenuation of guided light in a waveguide-based SPR-refractometer can reach several orders of magnitude and its transmission is most conveniently expressed in logarithmic units, it seems reasonable to characterize the width of the dip not by the conventional half-width, but rather by a full width at square root of the minimum (FWSRM) transmission value which corresponds to the half-width of the dip on a logarithmic scale. This width, as calculations show, is larger for higher SPM losses and smaller intersection angle of the dispersion curves of SPM and the waveguide mode.

The depth of the dip depends primarily on the length of the metallized section L. The best resolution is achieved with the deepest resonant dip, but if its depth exceeds the dynamic range of the spectrum analyzer employed, the shape of the dip can be distorted by noise. With this in mind we choose the length of the sensing section, in all cases, so that the attenuation at resonance is ∼80 dB, which corresponds roughly to the dynamic range of a modern optical spectrum analyzer (such as Yokogawa AQ6370D).

To compare metrological performance of different refractometric configuration we thus use the so-called Figure-of-Merit (FOM) parameter defined as the ratio of spectral sensitivity to the logarithmic half-width of the resonant dip. Refractometric resolution is inversely proportional to FOM [6] so the best

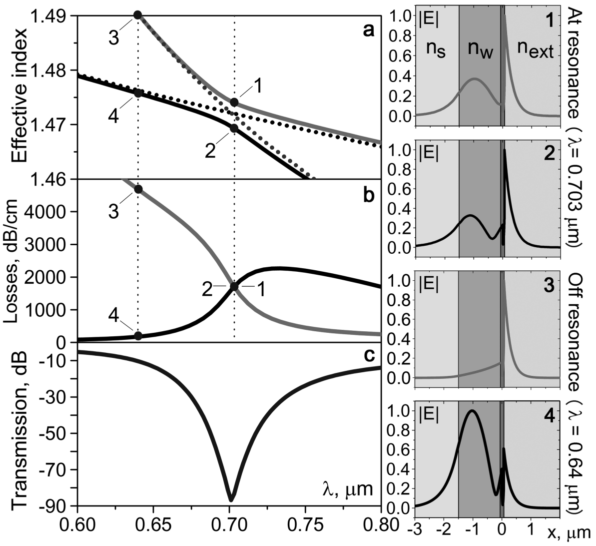

Fig. 2. Spectral dependencies of the effective refractive index (a) and losses (b) of the hybrid modes of the metallized section, as well as the transmission spectrum of the refractometer (c) at $th_m = 60$ nm, $n_{ext} = 1.4$, $L = 500\ \mu m$ .The insets show MMLS profiles at resonance ($\lambda = 0.703\ \mu m$, insets 1, 2) and off resonance ($\lambda = 0.64\ \mu m$, insets 3, 4).

SPR-refractometer with the minimum resolution is the one with the largest FOM value.

Another parameter of an SPR-refractometer, which is important for bio- and chemosensing applications, is the penetration depth (d_{SP}) of the surface plasmon mode into the ambient medium conventionally defined at the 1/e level of the SPM intensity profile. That is because the thickness of the sensing layer of ligand molecules (d_{lig}) can be much smaller than d_{sp}. In this case an SPR-refractometer is more appropriately characterized by the so-called local sensitivity: $S_{loc} \propto S_{RI} \frac{d_{lig}}{d_{SP}}$, which takes proper account of the sensitivity of SPM's propagation constant to refractive index variations in a thin layer near the metal film [6]. It then follows that refractometric resolution with respect to local RI variations should be proportional to the "local resolution coefficient" (LRC) defined as the ratio of d_{SP} to FOM, which we shall use to compare different SPR-refractometers in terms of local resolution – the smallest LRC value corresponds to the best configuration.

III. Results

A. SPR-Refractometer Without a Buffer Layer

In practical terms it is advantageous to build an SPR-refractometer with the most common and readily available optical materials, so let us choose SiO_2 ($n_s \sim 1.45$ [20]) as a substrate material and PMMA ($n_w \sim 1.49$ [22]) as a waveguiding layer material. Numerical calculations then show that for the waveguiding layer thickness $th_w = 1.5\ \mu m$ and ambient refractive index $n_{ext} = 1.4$ the dispersion curves of the separately considered waveguide and bulk surface plasmon modes intersect in the near infrared spectral range (Fig. 2a, dotted lines). By the separately considered BSPM we mean the mode of the metal film localized at metal | ambient medium interface, with the metal film being bounded on one side by the semi-infinite

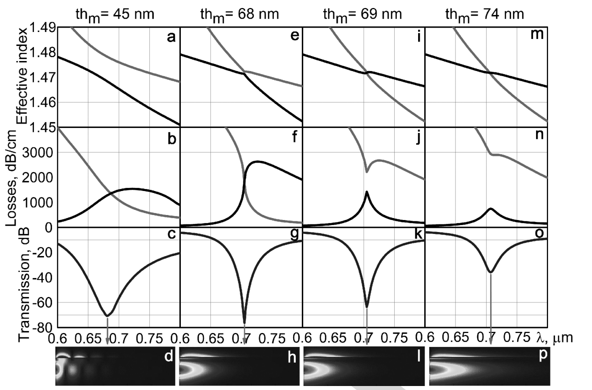

Fig. 3. Effective index and loss spectra of hybrid MMLS, transmission spectra of the refractometer, and electric field amplitude distribution in the metallized section at the resonant wavelength at $n_{ext} = 1.4$, $L = 500\ \mu m$ and $th_m = 45$ nm (a), (b), (c), (d), 68 nm (e), (f), (g), (h), 69 nm (i), (j), (k), (l), 74 nm (m), (n), (o), (p).

ambient medium and, on the other side, by semi-infinite dielectric with refractive index n_w. By the separately considered waveguide mode (WM) we mean the single fundamental mode of the waveguiding layer bounded by semi-infinite substrate and semi-infinite ambient medium.

According to the coupled mode theory, near the wavelength of intersection of WM and BSPM dispersion curves pronounced losses can occur in Section 2 as a result of transfer of guided light energy to surface plasmons, provided that the WM-BSPM coupling coefficient is sufficiently large. This is indeed the case for the metal film thickness $th_m = 60$ nm, which is confirmed by the results of calculation of the effective index spectra (Fig. 2a, solid lines), loss spectra (Fig. 2b) and profiles (insets 1-4) of the hybrid modes of multilayer structure (MMLS) forming Section 2. It is evident from insets 1 and 2 that at the resonant wavelength MMLS, with their profiles made up of the elements of both BSPM and WM, are indeed a result of the hybridization of the latter modes. Since both MMLS have similar profiles at this wavelength and, therefore, similar overlap integrals with the waveguide mode of Section 1, they are excited at the beginning of Section 2 with about the same amplitudes. Their losses are equally high (∼1700 dB/cm) and result in the attenuation of guided light power by ∼80 dB for the length of the metallized section L = 0.5 mm. Off the resonant wavelength, as seen from Fig. 2b and insets 3-4, both profiles and losses of MMLS are quite different. The low loss mode is closer in its profile to the waveguide mode of Section 1 and is, therefore, excited much more efficiently. As a result, there is no significant attenuation of light in Section 2 at this wavelength. It is in this way that a pronounced dip is formed in the transmission spectrum of the refractometer (Fig. 2c).

Numerical calculations show that, depending on the thickness of the metal film, the formation of the resonant dip can occur in two distinct scenarios. If the film thickness is 68 nm or less there is an anticrossing in the effective index spectra of hybrid MMLS, and a crossing in their loss spectra. This is illustrated by Fig. 2a, b ($th_m = 60$ nm) and Fig. 3a, b, e, f ($th_m = 45; 68$ nm). At film thicknesses of 69 nm or more, on the contrary, the MMLS spectra intersect, while their loss spectra do not (Fig. 3i, j, m, n ($th_m = 69, 74$ nm)).

These scenarios can be associated with two different coupling regimes between the separately considered WM and BSPM. The first scenario can be regarded as strong coupling whereby a periodic power exchange takes place at the resonant wavelength between the coupled modes (see also [23] for discussion and [24] for experimental observation of this). This is illustrated by the distribution of the electric field amplitude in Section 2 at a film thickness of 45 nm (Fig. 3d). From the point of view of the entire multilayer structure forming Section 2, this exchange corresponds to interference beats of hybrid MMLS with a period of $\lambda/\Delta n$, where Δn is the difference in their effective indexes at the resonant wavelength. Note that this period increases with increasing film thickness and, for example, at $th_m = 68$ nm, it becomes larger than the characteristic attenuation length of guided light in Section 2. In this case, the exchange of power between WM and BSPM proceeds too slowly to be seen against the background of the overall attenuation of light in Section 2 (Fig. 3h, $th_m = 68$ nm).

The second hybridization scenario can be associated with a weak-coupling regime in which such a periodic power exchange between the waveguide and surface plasmon modes at the resonant wavelength does not occur (see [24] for experimental observation of this regime). In terms of MMLS, this corresponds to a situation where interference beats between them are not possible due to their propagation constants being equal at $\lambda = \lambda_{SPR}$ (Fig. 3i, m).

We must emphasize that the terms "strong" and "weak" coupling are understood here differently than in the context of coupling between lossless modes, and both apply to the resonant wavelength where the real parts of the propagation constants of the coupled modes are exactly equal.

It follows from the coupled mode theory [21] that the coupling regime between WM and BSPM is determined by whether or not the coupling coefficient D is larger than the difference of their effective indexes. At the resonant wavelength the latter reduces, due to WM being lossless, to the imaginary part of the BSPM effective index n''_{SP}. If $D > n''_{SP}$, the dependences of the coupled modes amplitudes on the coordinate along the fiber can be shown to be quasiperiodic, which corresponds to the strong-coupling regime, and for $D < n''_{SP}$ they acquire a quasi-exponential character corresponding to the weak coupling regime.

The coupling coefficient is defined primarily by the thickness of the metal film: for larger th_m the profiles of WM and BSPM overlap less effectively which leads to lower D value and, therefore, weaker coupling. If the coupling becomes too weak ($D << n''_{SP}$), say at $th_m = 74$ nm, the transfer of guided light energy to surface plasmons becomes inefficient which considerably reduces the depth of the resonant dip (Fig. 3o). In terms of MMLS it is explained by the fact that their profiles and losses at the resonant wavelength differ, with lower loss MMLS being closer in its profile to the fundamental mode of Section 1. It is, as a result, excited more effectively and to a greater extent affects the overall transmission of the structure, which leads to the observed reduction of the depth of the dip.

On the other hand, if the coupling is too strong ($D >> n''_{SP}$), for example, at $th_m = 45$ nm, the spectral range around λ_{SPR} where the transfer of energy to surface plasmons is effective gets wider, which leads to the broadening of the resonant dip (Fig. 3c). We thus conclude that the sharpest resonant dip is obtained with the critical coupling - just at the border between weak and strong coupling regimes. At $n_{ext} = 1.4$ this is achieved with a film thickness of 68 nm (Fig. 3g).

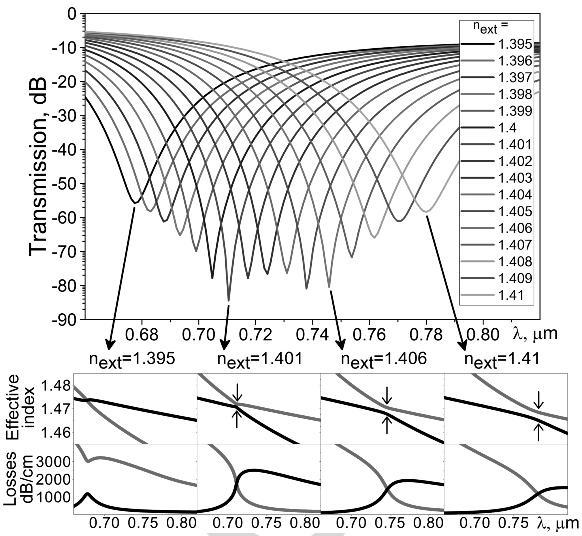

Fig. 4. Calculated transmission spectra of the refractometer for $n_{ext} =$ 1.395–1.41, $th_m = 68$ nm, L = 0.5 mm. Shown in the insets below are the effective index and loss spectra of MMLS of Section 2 at $n_{ext} =$ 1.395; 1.401; 1.406; 1.41.

The ambient refractive index, however, does not remain constant in the course of refractometric measurements. Its variation shifts the resonant wavelength, which, for a fixed value of th_m, is inevitably accompanied by changes in the resonant dip contrast. This is illustrated in Fig. 4 depicting transmission spectra of the refractometer calculated for $th_m = 68$ nm, $n_{ext} =$ 1.395–1.41, L = 0.5 mm. As evident from the dispersion curves of hybrid MMLS shown in the insets at the bottom of Fig. 4 the coupling between WM and BSPM gets stronger with increasing n_{ext} and λ_{SPR}. This is explained by the fact that, firstly, the profiles of WM and BSPM broaden as the wavelength increases and overlap more effectively thus leading to a larger coupling coefficient. Secondly, n''_{SP} value responsible for the losses of BSPM tend to decrease with increasing wavelength [6], which also makes the coupling stronger.

Thus the depth of the resonant dip first gradually growths while shifting from left to right with increasing n_{ext} as the coupling gets stronger but is still in the weak coupling regime ($n_{ext} < 1.4$). The switching to the strong coupling regime occurs at $n_{ext} \sim 1.4$ after which the coupling continues to grow stronger as seen from the growing difference in the effective indexes of MMLS at the resonant wavelength (marked with arrows in the insets of Fig. 4). At $n_{ext} > 1.4$ one can also observe slight quasiperiodic variations in the depth of the resonant dip. They arise from the periodic power exchange between the waveguide and surface plasmon modes resulting into the guided light, depending on the period of the exchange, being predominantly localized at the end of Section 2 either in the region of the waveguiding layer or near the metal film. This affects the transmission loss between Sections 2 and 3, which varies as the

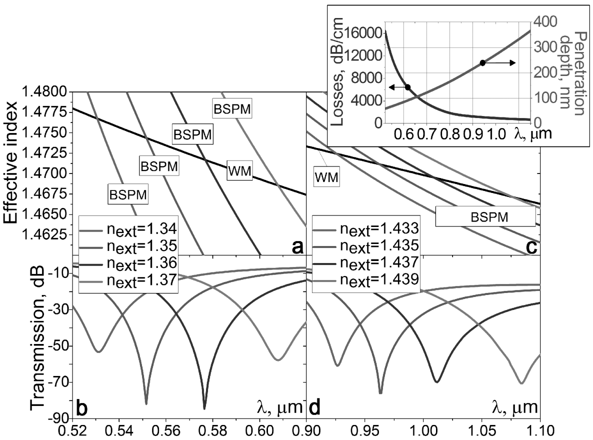

Fig. 5. Effective index spectra for the separately considered waveguide and bulk surface plasmon modes as well as transmission spectra of the refractometer at $th_m = 58$ nm, $th_w = 1\ \mu$m, L = 0.2 mm, $n_{ext} = 1.34$–1.37 (a), (b) and at $th_m = 75$ nm, $th_w = 2.5\ \mu$m, L = 1.3 mm, $n_{ext} = 1.433$–1.439 (c), (d). The upper-right inset shows the spectral dependences of losses and depth of penetration of BSPM into the ambient medium.

period of the exchange gets shorter with stronger coupling, thus leading to the observed variations in the depth of the dip.

When the ambient refractive index exceeds ~1.406 the resonant dip broadens due to WM-BSPM coupling becoming overly strong and its depth decreases due to lower losses of BSPM at longer wavelengths.

It then seems reasonable to define a range of efficient refractometric measurements (Δn_{ext}) as the range of n_{ext} values for which the depth of the resonant dip is less than the maximum depth by not more than an arbitrary threshold value, say 20 dB. For the configuration under study, as seen from Fig. 4, this corresponds roughly to n_{ext} ranging from 1.395 to 1.41, i.e., $\Delta n_{ext} \cong 0.015$. It also follows from the analysis of the transmission spectra in Fig. 4 that the spectral sensitivity of the refractometer is $S_{RI} \cong 6800$ nm/ RI unit (RIU), logarithmic half-width of the dip in the middle of the measured n_{ext} range – FWSRM ≅ 25 nm. The penetration depth of BSPM into the ambient medium at λ ~ 700 nm is $d_{sp} \cong 120$ nm (see the inset of Fig. 5), which yields FOM ≅ 270 and LRC ≅ 0.44.

It should be noted that the SPR-refractometer under consideration can be used for measuring other values of ambient refractive index, both higher and lower than 1.4. For example, at $n_{ext} \sim 1.35$ the phase-matching condition between the waveguide and surface plasmon modes is fulfilled near λ = 550 nm (Fig. 5a). The optimal film thickness in this case is 58 nm. For the waveguide layer to remain in the single-mode regime its width is reduced to 1 micron. Since the losses of BSPM in this spectral range are several times higher than those at λ ~ 700 nm (inset of Fig. 5) we also reduce the length of the metallized section to 0.2 mm.

In spite of the higher losses of BSPM the width of the resonant dip turns out in this case to be less than in the previous one: FWSRM ≅ 16 nm (at $n_{ext} \cong 1.35$), which can be explained by a much larger angle of intersection of WM and BSPM dispersion curves (Fig. 5a). It is for the same reason that, although physical sensitivity of BSPM's effective index to the ambient RI is larger at shorter wavelengths [6], the overall spectral sensitivity turns out in this case to be about 2.5 times lower than that at λ ~ 700 nm: $S_{RI} \cong 2600$ nm/RIU due to a drop in the instrumental sensitivity. The rage of measured refractive index is correspondingly larger: $\Delta n_{ext} \cong 0.03$. FOM amounts to ~162 which is more than 1.5 times worse than in the previous case. The penetration depth of BSPM into the ambient medium, however, at λ ~ 550 nm is only ~70 nm (inset of Fig. 5), so in terms of the local resolution there is virtually no difference from the previous case: LRC ≅ 0.43.

At a higher value of the ambient refractive index: $n_{ext} \sim 1.435$ the phase-matching condition between the waveguide and surface plasmon modes is fulfilled at λ ~ 1000 nm (Fig. 5c). The optimal waveguide width and metal film thickness in this case are 2.5 μm and 75 nm, respectively. The losses of BSPM in this spectral range are much lower than at λ ~ 700 nm or λ ~ 550 nm, so to get a ~80 dB resonant dip the length of the metallized section has to be extended to L = 1.3 mm. Secondly, the dispersion curves of WM and BSPM intersect here at a much smaller angle than in both cases considered above. This leads to a much higher spectral sensitivity due to a larger instrumental contribution: $S_{RI} \cong 26000$ nm/ RIU, narrowing of the measured RI range: $\Delta n_{ext} \cong 0{,}008$, and broadening of the resonant dip. The latter feature is, however, partially compensated by the lower losses of BSPM in this spectral range resulting in FWSRM ≅ 44 nm (at $n_{ext} \cong 1.435$). There is thus a significant advantage in terms combination of spectral sensitivity and width of the dip as compared to the previous cases: FOM ≅ 590. The local resolution is, however, virtually unchanged because of much deeper penetration of BSPM into the ambient medium at λ ~ 1000 nm ($d_{SP} \cong 270$ nm, inset of Fig. 5): LRC ≅ 0.46.

B. SPR-Refractometer Based on Symmetric (Long-Range) Surface Plasmon Mode

Introduction of a buffer layer between the waveguide and metal film with the refractive index close to that of the ambient medium enables one to build an SPR-refractometer both on symmetric (long-range) and antisymmetric (short-range) surface plasmon modes [6]. SSPM and ASPM differ significantly in their properties both from each other and from the bulk surface plasmon mode considered above. The metrological parameters of corresponding SPR-refractometers can, therefore, be widely different as well. To gain a benefit in metrological performance one must to the fullest possible extent exploit the advantages that a particular plasmon mode has to offer in terms of building an SPR-refractometer.

As for the long-range surface plasmon mode its major strength is in its low propagation losses [6], [15]–[17]. This enables one to obtain a reasonably narrow resonant dip even with a very small intersection angle between WM and SSPM dispersion curves, which may yield a very high spectral sensitivity due to a large instrumental contribution. The losses of SSPM tend to decrease for larger wavelength and thinner metal film [6], which makes it reasonable to use a long-wavelength spectral range and a thin metal film. Making the film too thin, however, is not practical and can be technologically challenging. At too long a wavelength, on the other hand, the intersection angle can become too small to produce a distinct resonant dip

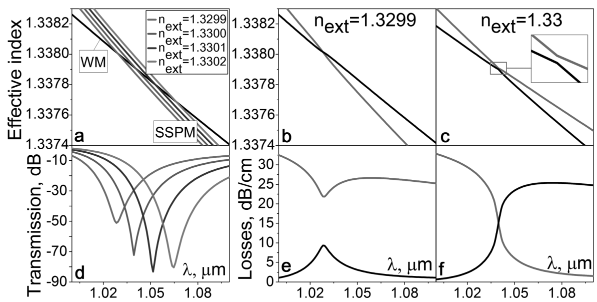

Fig. 6. Dispersion curves of the separately considered waveguide and symmetric surface plasmon modes (a) and transmission spectra of the SSPM-based refractometer (d) for $n_{ext} = 1.3299$–1.3302; effective index and loss spectra of the hybrid MMLS of the metallized section for $n_{ext} = 1.3299$ (b), (e) and 1.33 (c), (f) (L = 60 mm, $th_w = 200$ nm, $th_b = 13.3\ \mu$m, $th_m = 20$ nm).

in spite of SSPM's low losses. With thus choose as a compromise $th_m = 20$ nm and $\lambda \sim 1000$ nm. We note also that the effective index of the long-range surface plasmon mode is much lower than those of ASPM and BSPM, so to phase-match it to the waveguide mode one has to use materials with low optical density. The specified requirements are fulfilled e.g., with the following waveguiding structure: substrate made of Cytop polymer ($n_s \sim 1.34$ [25]), waveguiding layer – MgF_2 ($n_w \sim 1.37$ [26], $th_w = 200$ nm), buffer layer – Cytop, silver film ($th_m = 20$ nm).

Fig. 6a shows the dispersion curves of the separately considered WM and SSPM calculated for the chosen structure at $n_{ext} = 1.33$. As seen from the figure the phase-matching between the two modes can be achieved near $\lambda = 1040$ nm. To ensure the maximum contrast of the resonant dip we also require the switching from the weak to strong regime of WM-SSPM coupling to occur around this wavelength. Unlike the previously considered configuration, in the SPR-refractometer with a buffer layer it is the thickness of the buffer layer that is primarily responsible for the coupling regime. Calculation show that the optimal value of th_b at which the switching of coupling regimes occurs near $\lambda = 1040$ at $n_{ext} \cong 1.33$ amounts to 13.3 microns (Fig. 6b, c, e, f).

The transmission spectra of the refractometer calculated for $n_{ext} = 1.3299$–1.3302, $th_b = 13.3\ \mu$m are shown in Fig. 6d. One can conclude from the figure that spectral sensitivity in this case amounts to as high as ~120000 nm/RIU, $\Delta n_{ext} \cong 0{,}0004$, FWSRM $\cong$ 18 nm (at $n_{ext} \cong 1.3301$), i.e., FOM $\cong$ 6670, which is more than an order of magnitude higher than that of the SPR-refractometer without a buffer layer. In spite of the penetration depth of SSPM into the ambient medium being much higher than that of BSPM ($d_{SP} \cong 580$ nm at $\lambda \sim 1050$ nm) in terms of local resolution the SPR-refractometer based on SSPM has a significant advantage as well: LRC $\cong$ 0.09 which is ~5 times below that of SPR-refractometer without a buffer layer. We must note, however, that the advantage in metrological performance arises from the low losses of SSPM (~30 dB/cm at $\lambda \sim 1050$ nm) and it comes, therefore, at a cost of extending the length of the sensing section: an ~80dB resonant dip is achieved with the sensing section being as long as 6 cm.

If needed the sensing section can be shortened by choosing the parameters of the structure so that the SPR condition is fulfilled at a shorter wavelength where SSPM has higher losses. For example, at $th_w = 400$ nm and $n_{ext} = 1.33$ the waveguide mode is phase-matched to SSPM at around $\lambda = 600$ nm. The optimal thickness of the buffer layer is $th_b = 2.6\ \mu$m. The losses of SSPM in this spectral range are about an order of magnitude higher than those at $\lambda \sim 1000$ nm: ~310 dB/cm enabling 10-fold shortening of the sensing section: L = 6 mm. The spectral sensitivity, however, turns out in this case to be only about a tenth of that at $\lambda \sim 1000$ nm due to a sharp drop in the instrumental contribution: $S_{RI} \cong$ 16000 nm/ RIU, which is accompanied by broadening of the RI measurement range: $\Delta n_{ext} \cong 0.003$ and some narrowing of the resonant dip: FWSRM $\cong$ 12 nm. Thus, in terms of combination of sensitivity and resonant dip width such a configuration is more than 5 times inferior to the previous one: FOM $\cong$ 1330. The local resolution is, however, not much worse than that in the previous case due to much a lower penetration depth of SSPM at $\lambda \sim 600$ nm than at $\lambda \sim 1000$ nm ($d_{sp} \cong 200$ nm): LRC $\cong$ 0.15.

C. SPR-Refractometer Based on the Antisymmetric (Short-Range) Surface Plasmon Mode

From the analysis of the properties of the antisymmetric surface plasmon mode [6] one can conclude that its main advantages in terms of building an SPR refractometer are as follows. Firstly, it has a higher degree of field localization near the film which may lead to better sensitivity to local variations of refractive index. Secondly, it has a higher physical sensitivity to the ambient refractive index as compared to SSPM. Thirdly, higher losses of ASPM allow one to obtain a deep resonant dip with a very short sensing section, which aids in miniaturization of the refractometer. All of these features become more pronounced with decreasing wavelength and metal film thickness [6]. Another circumstance to take into account is that, as calculations show, when the media on two sides of the film differ in refractive indexes the profile of ASPM tends to shift to the optically denser medium, which brings about additional increase in sensitivity to the refractive index of that medium. Thus in order to exploit ASPM's advantages to the fullest degree one should use shorter wavelength range, very thin film and make the refractive index of the buffer layer somewhat lower than that of the ambient medium. Due to the effective index of ASPM being quite high [6], to enable its phase-matching with the waveguide mode one should use for the waveguiding layer a high optical density material.

The stated requirements are satisfied e.g., with the following structure: substrate – SiO_2, waveguiding layer – Si_3N_4 ($n_w \sim 2$ [27], $th_w = 250$ nm), buffer layer – Teflon AF2400 ($n_b \sim 1.28$ [28]), silver film ($th_m = 20$ nm), ambient medium ($n_{ext} > n_b$).

Fig. 7a shows the dispersion curves of the separately considered waveguide and antisymmetric plasmon modes calculated for the chosen structure at different n_{ext} values in the range 1.34–1.37. As one can see, the SPR condition is fulfilled at $\lambda \sim 640$ nm where ASPM losses are found to be as high as ~42000 dB/cm. The optimal thickness of the buffer layer at which the switching of WM-ASPM coupling regimes occurs near this wavelength is $th_b = 180$ nm (Fig. 7b, c, e, f). The losses of hybrid MMLS at the resonant wavelength reach

TABLE I
SPECIFICATIONS OF THE SPR-REFRACTOMETERS UNDER STUDY

	SPR-refractometer without a buffer layer			SPR-refractometer based on long-range surface plasmon mode		SPR-refractometer based on short-range surface plasmon mode	
Measured RI, $\overline{n_{ext}} \pm \frac{\Delta n_{ext}}{2}$	1.355±0.015	1.404±0.0075	1.437±0.004	1.33±0.0015	1.3301±0.0002	1.355±0.015	1.33±0.01
Resonant wavelength range, nm	530-610	680-780	920-1120	600-650	1030-1080	625-655	900-980
Instrumental sensitivity, S_1	2 000	6 000	24 000	34 000	316 000	825	4 350
Physical sensitivity, S_2	1.26	1.14	1.08	0.47	0.38	1.09	0.85
Spectral sensitivity S_{RI}, nm/RIU	**2 600**	**6 800**	**26 000**	**16 000**	**120 000**	**900**	**3 700**
FWSRM, nm	**16**	**25**	**44**	**12**	**18**	**35**	**65**
FOM	**162**	**270**	**590**	**1 330**	**6 670**	**25,7**	**57**
SPM losses near λ_{SPR}, dB/cm	11 620	3 650	970	310	30	42 000	11 000
Length of the sensing section, mm	**0.2**	**0.5**	**1.3**	**6**	**60**	**0.04**	**0.18**
SPM penetration, d_{SP}, nm	70	120	270	200	580	44	117
Local resolution coefficient, LRC	**0.43**	**0.44**	**0.46**	**0.15**	**0.09**	**1.7**	**2.05**

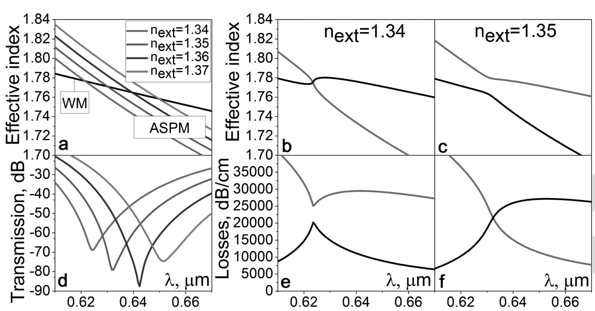

Fig. 7. Dispersion curves of the separately considered waveguide and antisymmetric surface plasmon modes (a), as well as transmission spectra of the ASPM-based refractometer (d) calculated for $n_{ext} = 1.34$–1.37; effective index and loss spectra of hybrid MMLS of the metallized section calculated for $n_{ext} = 1.37$ (b), (e) and 1.35 (c), (f) ($L = 0.04$ mm, $th_w = 250$ nm, $th_b = 180$ nm, $th_m = 20$ nm).

~22 000 dB/cm which makes it possible to reduce the length of the sensing section to just $L = 40$ μm.

The transmission spectra of the refractometer are shown in Fig. 7d. It can be concluded from the figure that the spectral sensitivity is in this case ~900 nm/RIU, $\Delta n_{ext} \cong 0.03$, FWSRM $\cong$ 35 nm (at $n_{ext} \cong 1.36$), and FOM $\cong$ 25.7, which is about an order of magnitude lower than the FOM of the refractometer without a buffer layer and 260 times lower than the FOM of the refractometer on SSPM. The penetration depth of ASPM into the ambient medium, however, at $\lambda \sim 640$ nm is just ~44 nm and LRC amounts, therefore, to ~1.7.

We note that such a low sensitivity results from an extraordinarily low instrumental contribution due to a very large intersection angle of WM and ASPM dispersion curves. The parameters of the waveguiding structure can be adjusted to shift the resonance to a longer wavelength thus decreasing the intersection angle and enhancing the sensitivity. This will also broaden the resonant dip but due to ASPM losses falling with wavelength some benefit should be expected in terms of FOM parameter (at the expense of a longer sensing section). For example, at $th_b = 150$ nm and $n_{ext} \sim 1.33$ the SPR condition is fulfilled at $\lambda \sim 900$ nm where the losses of ASPM amount to ~11000 dB/cm. At the optimal film thickness ($th_b = 568$ nm) an 80-dB resonant dip can be obtained with a sensing section of 180 μm. The spectral sensitivity is then found to be ~3700 nm/RIU, $\Delta n_{ext} \cong 0.02$, FWSRM $\cong$ 65 nm, $d_{SP} \cong$ 117 nm, which results in FOM $\cong$ 57 and LRC $\cong$ 2.05.

IV. DISCUSSION

The specifications of the studied BSPM, SSPM- and ASPM-based refractometers are summarized in Table I. As seen from the table the difference in metrological performance of different configurations results mainly from their spectral sensitivity. The physical sensitivity, however, does not change much and the observed variations are primarily due to the greatly varying instrumental contribution.

The best specifications are achieved with the SPR-refractometer based on symmetric or long-range surface plasmon mode: due to its low losses a sharp resonant dip can be obtained even with a very small intersection angle of WM and SSPM dispersion curves yielding an extremely high instrumental and hence overall spectral sensitivity. The advantage in terms of FOM parameter reaches about two orders of magnitude as compared to the ASPM-based SPR-refractometer and one order of magnitude as compared to the SPR-refractometer without a buffer layer.

Apart from its low losses the symmetric surface plasmon mode has a larger penetration depth into the ambient medium. In terms of local resolution, therefore, the advantage of using SSPM instead of ASPM or BSPM is less pronounced: LRC is about 20 times lower than that for ASPM and ~6 times lower than that for BSPM.

We should also emphasize that the advantage in metrological performance of the SPR-refractometer based on symmetric surface plasmon mode comes at a cost of extending the length of the metallized section: to obtain a resonant dip of the same depth as in ASPM- and BSPM-based refractometers a much longer (up to three orders of magnitude) sensing section is required.

The most compact sensing element with the minimum length of the sensing section is characteristic of the SPR-refractometer based on the antisymmetric surface plasmon mode. It has, however, the worst metrological performance among all the studied configurations due to the enormous losses of ASPM.

The SPR-refractometer without a buffer layer occupies an intermediate position between those based on SSPM and ASPM, both in terms of metrological performance and sensing section length. It has, however, an important practical advantage of having the simplest structure, which facilitates the fabrication process.

One can also conclude from the table that the values of measured refractive index depend both on the parameters of the metallized section and on the working spectral range. By choosing a longer wavelength range where a surface plasmon mode has lower losses (and using a longer sensing section) one can obtain higher metrological performance in terms of FOM parameter. The local resolution coefficient, however, does not change much since the increase in FOM is offset by a higher penetration depth of SPM into the ambient medium. We also note that if the resonant wavelength is shifted too far into the infrared ($\lambda_{SPR} \gtrsim$ 1200 nm) the intersection angle between WM and SPM dispersion curves may get so small that refractometric measurements, in spite of a very high sensitivity, become no longer possible due to smearing out of the resonant dip.

In closing, we emphasize that metrological parameters summarized in Table I have been obtained in the 2D-geometry approximation and depend on the specific choices of materials and geometric parameters of the refractometers. Their primary purpose is, therefore, not to characterize performance of practical SPR-sensors but to illustrate in a quantitative manner the relative merits of refractometers based on bulk, symmetric and antisymmetric surface plasmon modes. The revealed patterns and relationships, we believe, are also valid in 3D geometry and do not depend on the specific details of the refractometers.

V. Conclusions

We have thus studied three SPR-refractometer configurations: without a buffer layer based on the excitation of the bulk surface plasmon mode, and with a buffer layer using symmetric (long-range) and antisymmetric (short-range) surface plasmon modes. It is shown the highest metrological performance is achieved with the symmetric SPM, which, however, requires a much longer sensing section. If miniaturization of the sensor is of utmost importance the preferred type of plasmon mode to use is the antisymmetric one, which enables minimization of the sensing section length at a cost of impaired metrological specifications. Finally, in terms of ease of fabrication the most attractive configuration is that without a buffer layer, which is intermediate between SSPM- and ASPM-based refractometers both in terms of metrological performance and sensing section length.

References

[1] A. Rasooly and K. E. Herold, *Biosensors and Biodetection*. New York, NY, USA: Humana, 2009.

[2] Ligler F. S. and C. R. Taitt, *Optical Biosensors: Today and Tomorrow*. Amsterdam, The Netherlands: Elsevier, 2011.

[3] F. Baldini *et al.*, *Optical Chemical Sensors*. Berlin, Germany: Springer Science & Business Media, 2006, vol. 224.

[4] X. Guo and J. Biophoton,“Surface plasmon resonance based biosensor technique: A review,” *J. Biophoton.*, vol. 5, pp. 483–501, 2012.

[5] J. Homola, “Surface plasmon resonance sensors for detection of chemical and biological species,” *Chem. Rev.*, vol. 108, no. 2, pp. 462–493, 2008.

[6] J. Homola, *Surface Plasmon Resonance Based Sensors*. Berlin, Germany: Springer-Verlag, 2006.

[7] B. D. Gupta and R. K. Verma “Surface plasmon resonance-based fiber optic sensors: Principle, probe designs, and some applications,” *J. Sensors*, vol. 2009, 2009, Art. no. 979761.

[8] R. Kashyap and G. Nemova, “Surface plasmon resonance-based fiber and planar waveguide sensors,” *J. Sensors*, vol. 2009, 2009, Art. no. 645162.

[9] C. Caucheteur, T. Guo, and J. Albert “Review of plasmonic fiber optic biochemical sensors: Improving the limit of detection,” *Analytical Bioanalytical Chem.*, vol. 407, no. 14, pp. 3883–3897, 2015.

[10] E. Klantsataya *et al.*, “Plasmonic fiber optic refractometric sensors: From conventional architectures to recent design trends,” *Sensors*, vol. 17, no. 1, 2016, Art. no. 12.

[11] S. K. Srivastava and B. D. Gupta, “Fiber optic plasmonic sensors: Past, present and future,” *Open Optics J.*, vol. 7, no. 1, pp. 58–83, 2013.

[12] M. E. Bosch *et al.*, “Recent development in optical fiber biosensors,” *Sensors*, vol. 7, no. 6, pp. 797–859, 2007.

[13] A. V. Dyshlyuk *et al.*, “Numerical and experimental investigation of surface plasmon resonance excitation using whispering gallery modes in bent metal-clad single-mode optical fiber,” *J. Lightw. Technol.*, vol. 35, no. 24, pp. 5425–5431, Dec. 2017.

[14] Y.-S. Chu *et al.*, “Surface plasmon resonance sensors using silica-on-silicon optical waveguides,” *Microw. Opt. Technol. Lett.*, vol. 48, no. 5, pp. 955–957, 2006.

[15] G. G. Nenninger *et al.*, “Long-range surface plasmons for high-resolution surface plasmon resonance sensors,” *Sensors Actuators B: Chem.*, vol. 74, no. 1–3, pp. 145–151, 2001.

[16] R. Slavík and J. Homola, “Ultrahigh resolution long range surface plasmon-based sensor,” *Sensors Actuators B: Chem.*, vol. 123, no. 1, pp. 10–12, 2007.

[17] J. Dostálek, A. Kasry, and W. Knoll, “Long range surface plasmons for observation of biomolecular binding events at metallic surfaces,” *Plasmonics*, vol. 2, no. 3, pp. 97–106, 2007.

[18] B. Fan, F. Liu, Y. Li, Y. Huang, Y. Miura, and D. Ohnishi, “Refractive index sensor based on hybrid coupler with short-range surface plasmon polariton and dielectric waveguide,” *Appl. Phys. Lett.*, vol. 100, no. 11, 2012, Art. no. 111108.

[19] B. Fan *et al.*, “Integrated refractive index sensor based on hybrid coupler with short range surface plasmon polariton and dielectric waveguide,” *Sensors Actuators B: Chem.*, vol. 186, pp. 495–505, 2013.

[20] E. D. Palik *Handbook of Optical Constants of Solids*. New York, NY, USA: Academic, 1998.

[21] A. W. Snyder and J. Love *Optical Waveguide Theory*. Berlin, Germany: Springer Science & Business Media, 2012.

[22] N. Sultanova, S. Kasarova, and I. Nikolov, “Dispersion properties of optical polymers,” *Acta Physica Polonica-Series A Gen. Phys.*, vol. 116, no. 4, pp. 585–587, 2009.

[23] M. L. Nesterov, A. V. Kats, and S. K. Turitsyn, “Extremely short-length surface plasmon resonance devices,” *Optics Express* vol. 16, no. 25, pp. 20227–20240, 2008.

[24] H. Ditlbacher *et al.*, “Coupling dielectric waveguide modes to surface plasmon polaritons,” *Opt. Express*, vol. 16, no. 14, pp. 10455–10464, 2008.

[25] 2018. [Online]. Available: http://www.bellexinternational.com/products/cytop/pdf/cytop-catalog.pdf

[26] H. H. Li, “Refractive index of alkaline earth halides and its wavelength and temperature derivatives,” *J. Phys. Chem. Ref. Data*, vol. 9, no. 1, pp. 161–290, 1980.

[27] H. R. Philipp, “Optical properties of silicon nitride,” *J. Electrochemical Soc.*, vol. 120, no. 2, pp. 295–300, 1973.

[28] M. K. Yang, R. H. French, and E. W. Tokarsky, “Optical properties of Teflon AF amorphous fluoropolymers,” *J. Micro/Nanolithography, MEMS, MOEMS*, vol. 7, no. 3, 2008, Art. no. 033010.

Authors’ biographies not available at the time of publication.